

Strongly-coupled Josephson junction array for simulation of frustrated one-dimensional spin models

Liang-Hui Du, Xingxiang Zhou,* Yong-Jian Han, Guang-Can Guo, and Zheng-Wei Zhou†
*Key Laboratory of Quantum Information and Department of Optics and Optical Engineering,
 University of Science and Technology of China, Chinese Academy of Sciences, Hefei, Anhui 230026, China*
 (Dated: October 31, 2018)

We study the capacitance-coupled Josephson junction array beyond the small-coupling limit. We find that, when the scale of the system is large, its Hamiltonian can be obtained without the small-coupling approximation and the system can be used to simulate strongly frustrated one-dimensional Ising spin problems. To engineer the system Hamiltonian for an ideal theoretical model, we apply a dynamical decoupling technique to eliminate undesirable couplings in the system. Using a 6-site junction array as an example, we numerically evaluate the system to show that it exhibits important characteristics of the frustrated spin model.

PACS numbers: 03.67.Ac, 75.10.Jm, 85.25.Cp

I. INTRODUCTION

As an important application of quantum information science, quantum simulation of difficult physics problems has received much attention in recent years. Theoretically, there have been many proposals of quantum simulators based on various physical systems [1–5]. Experimentally, simulations of some important physics models have been demonstrated [6–11].

Quantum simulation is most valuable for studying strongly correlated problems since there are no generally-applicable theoretical methods to solve them. The strong interactions involved in these problems usually translate into strong couplings between entities in a quantum simulator. This requirement of strong couplings often poses a challenge for the design and construction of a quantum simulator, since it can be difficult to engineer such couplings in a simulation system. Even when strong couplings are available, it can still be nontrivial to tailor the couplings in a well-controlled manner that is required for the problems to be simulated. As one such example, it is usually difficult to obtain the system Hamiltonian for a Josephson junction array when the couplings between the junctions are strong. Consequently, Josephson device based quantum simulation systems often operate in the small coupling limit in which the system Hamiltonian can be obtained by treating the coupling as perturbation [12–14].

In order to go beyond the small-coupling limit and construct a system useful for simulating strongly correlated physics, in this paper we investigate a one-dimensional Josephson junction array which is coupled by large capacitances that cannot be treated perturbatively. Interestingly, the system Hamiltonian can be obtained exactly without the small coupling approximation. It is found that, in the large coupling limit, the interaction strength

between next nearest neighbors can become comparable with that between the nearest neighbors. Because of this, we can use the system to study the important problem of one-dimensional frustrated spin models whose phase diagrams and properties have not been completely resolved [15–19]. In order to control the system Hamiltonian to match that of the ideal theoretical model, we use a dynamical decoupling technique to suppress interactions between neighbors that are three site locations or farther apart.

II. SYSTEM HAMILTONIAN OF THE JOSEPHSON-JUNCTION ARRAY

The system we study is an N -site Josephson junction array as shown in Fig. 1. Each site consists of a charge island biased by a voltage source V_{gi} through a gate capacitance C_{gi} , where $i = 1, \dots, N$. The charge on the island can tunnel through a SQUID device whose total capacitance is C_J and whose effective Josephson energy \mathcal{E}_J can be adjusted by a flux bias. Adjacent charge islands, as well as those at the ends of the array, are coupled by a capacitance C_c . We take the average phase φ_i of the SQUID on site i as the generalized coordinates for the system. Its rate of change is determined by the voltage V_j across the Josephson junction according to the Josephson relation $V_j = (\hbar/2e)\dot{\varphi}_i$ [20]. The charging energy T of the capacitances and the Josephson energy V of the junctions are

$$T = \frac{1}{2} \sum_{i=1}^N \left[\left(\frac{\hbar}{2e} \right)^2 C_J \dot{\varphi}_i^2 + C_{gi} (V_{gi} - \frac{\hbar}{2e} \dot{\varphi}_i)^2 \right. \\ \left. + C_c \left(\frac{\hbar}{2e} \right)^2 (\dot{\varphi}_i - \dot{\varphi}_{i+1})^2 \right]. \quad (1)$$

$$V = - \sum_i \mathcal{E}_J \cos \varphi_i. \quad (2)$$

From the Lagrangian $\mathcal{L} = T - V$ of the system, we can derive the generalized momentum which is related to the

*Electronic address: xizhou@ustc.edu.cn

†Electronic address: zwzhou@ustc.edu.cn

charge number on the islands

$$P_i = \partial \mathcal{L} / \partial \dot{\varphi}_i \equiv -\hbar n_i. \quad (3)$$

Denoting the charge number on the i th island n_i and the bias charge number $n_{gi} = C_{gi} V_{gi} / 2e$, we can write the system's equation of motion

$$\frac{\hbar}{(2e)^2} \mathbf{M} \vec{\varphi} = \vec{n}, \quad (4)$$

where $\vec{\varphi} = [\dot{\varphi}_1, \dot{\varphi}_2, \dots, \dot{\varphi}_i, \dots, \dot{\varphi}_N]^T$, $\vec{n} = [n_1 - n_{g1}, n_2 - n_{g2}, \dots, n_i - n_{gi}, \dots, n_N - n_{gN}]^T$, and \mathbf{M} is the matrix

$$\mathbf{M} = \begin{pmatrix} C_\Sigma & -C_c & \cdots & \cdots & \cdots & -C_c \\ -C_c & C_\Sigma & -C_c & \cdots & \cdots & 0 \\ 0 & -C_c & C_\Sigma & -C_c & \cdots & 0 \\ \cdots & \cdots & \cdots & \cdots & \cdots & \cdots \\ \cdots & \cdots & -C_c & C_\Sigma & -C_c & \cdots \\ -C_c & \cdots & \cdots & \cdots & \cdots & \vdots \end{pmatrix}, \quad (5)$$

where $C_\Sigma = C_J + C_{gi} + 2C_c$ is the total capacitance of each island.

The Hamiltonian of this Josephson junction array is:

$$\begin{aligned} H &= \sum_i P_i \dot{\varphi}_i - \mathcal{L} \\ &= \frac{1}{2} \left(\frac{\hbar}{2e} \right)^2 \vec{\varphi}^T \mathbf{M} \vec{\varphi} + V \\ &= \frac{1}{2} (2e)^2 \vec{n}^T \mathbf{M}^{-1} \vec{n} + V. \end{aligned} \quad (6)$$

In order to obtain the system Hamiltonian, the inverse matrix of \mathbf{M} must be calculated. Since it is nontrivial to exactly solve for \mathbf{M}^{-1} , most previous studies [12, 13] have assumed a small coupling capacitance C_c so the system Hamiltonian can be obtained by treating the coupling as perturbation. Unfortunately, this precludes the

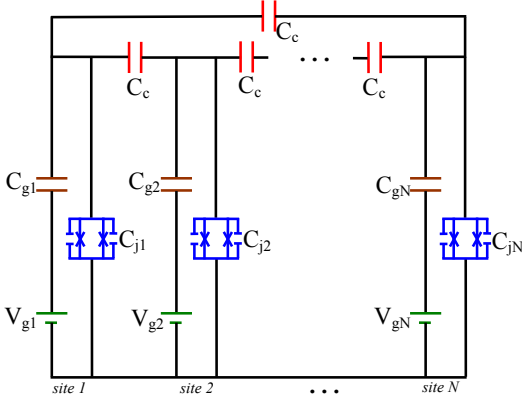


FIG. 1: (Color online) The capacitance-coupled Josephson junction array. C_c is the coupling capacitance between neighboring junctions. V_{gi} is the bias voltage and C_{gi} is the bias capacitance of the Josephson junction at site i . The total capacitance and Josephson energy are C_{ji} and \mathcal{E}_J .

system from being used to simulate strongly-correlated problems in which strong couplings are required. Here, we assume that C_c is not necessarily small and try to solve for \mathbf{M}^{-1} exactly.

Considering the translational symmetry of the problem, we see the inverse matrix \mathbf{M}^{-1} must be in the form

$$\mathbf{M}^{-1} = \begin{pmatrix} a_1 & a_2 & \cdots & a_{N/2+1} & \cdots & a_3 & a_2 \\ a_2 & a_1 & & & & & a_3 \\ \vdots & & \ddots & & & & \\ a_{N/2+1} & & & & & & \vdots \\ \vdots & & & & \ddots & & \\ a_3 & & & & & a_1 & a_2 \\ a_2 & & \cdots & & & a_2 & a_1 \end{pmatrix}, \quad (7)$$

Using some mathematic techniques for solving polynomials, we can calculate the values of the matrix elements in \mathbf{M}^{-1} exactly:

$$a_i = \frac{1}{C_\Sigma} (\lambda^{i-1} A_0 + \frac{1}{\lambda^{i-1}} B_0), \quad (8)$$

where

$$A_0 = \frac{1}{1 - 2\beta\lambda + (1 - \frac{2\beta}{\lambda}) \frac{2\beta - \lambda}{1 - 2\beta\lambda} \lambda^{N-1}}, \quad (9)$$

$$B_0 = \frac{(2\beta - \lambda) \lambda^{N-1}}{1 - 2\beta\lambda} A_0, \quad (10)$$

$$\lambda = \frac{1 - \sqrt{1 - 4\beta^2}}{2\beta}, \quad (11)$$

$$\beta = \frac{C_c}{C_\Sigma} = \frac{C_c}{2C_c + C_{gi} + C_J} < \frac{1}{2}. \quad (12)$$

When $N \rightarrow \infty$, the above results simplify to $A_0 \rightarrow 1/(1 - 2\beta\lambda)$, $B_0 \rightarrow 0$, and $a_i = \lambda^{i-1} A_0 / C_\Sigma$.

As can be seen in Eq. (6), λ characterizes the ratio between adjacent and non-adjacent interaction strengths in our system. According to Eqs. (11) and (12), λ is determined by the coupling capacitance C_c . In the

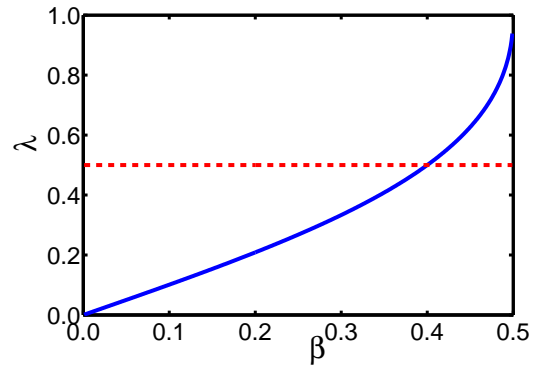


FIG. 2: (Color online) The relationship between λ and β . The dashed red line corresponds to $\lambda = 1/2$.

weak coupling limit $C_c \ll C_\Sigma$, $\beta \ll 1$ and λ is nearly equal to β . However, when the coupling is strong, λ increases quickly, as shown in Fig. 2. In particular, when the coupling capacitance C_c dominates, λ can approach 1, and the Hamiltonian in Eq. (6) describes a deeply frustrated system with appreciable non-adjacent interactions. Meanwhile, according to the results of Ref. [21], there exist many close energy levels as β approaches $1/2$ too closely, which can fail the two-level approximation. Therefore we only pay our attention to a large β , but not closely approaching $1/2$ in the rest of our paper.

Under proper conditions, if we bias the charge islands at the vicinity of $n_{gi} = 1/2$, we can use the two-level approximation for the charge qubits with $n_i = 0$ and $n_i = 1$ as the basis states. We can then write the system Hamiltonian in the following Pauli matrix representation

$$H_{JJA} = \sum_i \sum_j (-1)^j (\lambda)^{j-1} \sigma_i^z \sigma_{i+j}^z - B \sum_i \sigma_i^x, \quad (13)$$

where the spin up and down states represent the $n_i = 0$ and $n_i = 1$ states, and the transverse magnetic field $B = -\mathcal{E}_j C_\Sigma / (2\lambda e^2 A_0)$. B can be adjusted by tuning the magnetic flux of the SQUIDs. Here we applied a canonical σ^x transformation on even sites for the convenience of our following discussion about phase diagram without changing the physics of the system. Usually, two-level approximation works very well for a single Josephson charge island [22–24]. In our system of Josephson junction array, more careful analysis is necessary. Appendix A provides a detailed discussion about the applicability of the two-level approximation in our system.

III. SIMULATION OF THE ANNNI MODEL USING DYNAMICAL DECOUPLING

Our circuit is useful for quantum simulation of frustrated spin problems since it exhibits strong non-adjacent spin interactions in the large coupling limit. However, the Hamiltonian in Eq. (13) does not correspond to an ideal theoretical model with limited-range interactions yet. We intend to further engineer it for quantum simulation of well known frustrated models. As an example, we show how to simulate the one dimensional axial next-nearest-neighbor Ising (ANNNI) model in external fields. Its Hamiltonian is given by

$$H_{AI} = - \sum_i \sigma_i^z \sigma_{i+1}^z + \lambda \sum_i \sigma_i^z \sigma_{i+2}^z - B \sum_i \sigma_i^x. \quad (14)$$

The ANNNI problem is an important model for studying frustrated physics due to competition between adjacent and non-adjacent neighbor interactions [25, 26]. Despite years of research, its phase diagrams and physical properties have not been completely resolved [15–19].

Comparing our circuit Hamiltonian in Eq. (13) and target Hamiltonian in Eq. (14), we find that there are extra terms that describe interactions between spins that

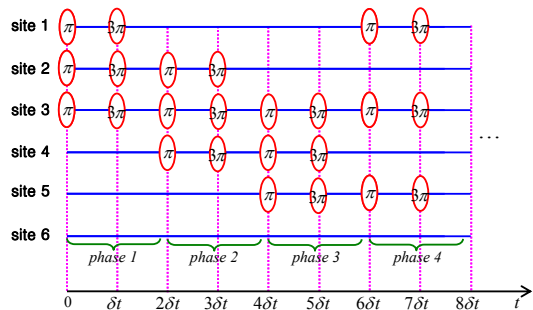


FIG. 3: (Color online) The dynamical decoupling control scheme to eliminate interactions between spins that are 3 sites apart. The ellipses in groups of 3 along the vertical direction represent simultaneous π or 3π pulses applied to the qubits.

are 3 or more sites apart. We eliminate these extra terms by using techniques of dynamical decoupling [27, 28]. In this practice, we apply carefully designed sequences of fast short pulses to individual qubits to engineer a Hamiltonian that can be very different than the original Hamiltonian.

In the following, we will demonstrate how to eliminate interactions between spins that are 3 sites apart for a spin chain with the Hamiltonian in Eq. (13). For clarification and ease of illustration, we discuss the details of our scheme on a 6-site spin chain with periodic boundary condition. The same technique applies in a spin chain with arbitrary length.

When the number of qubits in the system is 6, the Hamiltonian in Eq. (13) reads

$$\begin{aligned} H_s = & J_1(\sigma_1^z \sigma_2^z + \sigma_2^z \sigma_3^z + \sigma_3^z \sigma_4^z + \sigma_4^z \sigma_5^z + \sigma_5^z \sigma_6^z + \sigma_6^z \sigma_1^z) \\ & + J_2(\sigma_1^z \sigma_3^z + \sigma_2^z \sigma_4^z + \sigma_3^z \sigma_5^z + \sigma_4^z \sigma_6^z + \sigma_5^z \sigma_1^z + \sigma_6^z \sigma_2^z) \\ & + J_3(\sigma_1^z \sigma_4^z + \sigma_2^z \sigma_5^z + \sigma_3^z \sigma_6^z) - B \sum_{i=1}^6 \sigma_i^x \end{aligned} \quad (15)$$

where J_1 and J_2 are interaction strengths between the nearest and next-nearest neighbors and J_3 is that between spins that are 3 sites apart.

Our scheme to engineer the desired Hamiltonian involves applying rapid pulsed operations $R_x(\theta) = \exp\{-i\theta\sigma_x/2\}$ on individual qubits. When $\theta = \pi$ (3π) the corresponding unitary operation is $R_x(\pi) = -i\sigma^x$ ($R_x(3\pi) = R_x^\dagger(\pi) = i\sigma^x$). We have the following commutation relations:

$$R_x^\dagger(\pi)\sigma^z R_x(\pi) = -\sigma^z, \quad (16)$$

$$R_x^\dagger(\pi)\sigma^x R_x(\pi) = \sigma^x, \quad (17)$$

$$R_x^\dagger(\pi)e^{-i\hat{H}t} R_x(\pi) = e^{-i[R_x^\dagger(\pi)\hat{H}R_x(\pi)]t}. \quad (18)$$

Our procedure contains four phases as shown in Fig. 3. Each phase is completed in an interval of $2\delta t$ where δt is a short time. At the beginning of each phase, the operations $R_x^{(i,j,k)}(\pi) = R_x^i(\pi)R_x^j(\pi)R_x^k(\pi)$ ($i, j, k = 1, 2, \dots, 6$) are applied to the qubits on sites i, j , and k simultane-

ously (see Fig. 3). After a time interval of δt , the conjugate operations $R_x^{\dagger(1,2,3)}(\pi)$ are applied in the second half of the phase. The evolution of the system at the end of phase 1 is given by

$$U_1 = e^{-iH_s \delta t} R_x^{\dagger(1,2,3)}(\pi) e^{-iH_s \delta t} R_x^{(1,2,3)}(\pi). \quad (19)$$

For a short time duration δt , we have $e^{-iH_1 \delta t} e^{-iH_2 \delta t} = e^{-i(H_1+H_2)\delta t} + O(\delta t^2)$. To first order in δt , the unitary operator $U_1 = \exp(-iH_1^{eff} 2\delta t)$, where the effective Hamiltonian in phase 1 is

$$\begin{aligned} H_1^{eff} &= H_s + R_x^{\dagger(1,2,3)}(\pi) H_s R_x^{(1,2,3)}(\pi) \\ &= J_1(\sigma_1^z \sigma_2^z + \sigma_2^z \sigma_3^z + \sigma_4^z \sigma_5^z + \sigma_5^z \sigma_6^z) \\ &\quad + J_2(\sigma_1^z \sigma_3^z + \sigma_4^z \sigma_6^z) - B \sum_{i=1}^6 \sigma_i^x. \end{aligned} \quad (20)$$

From Eq. (20), we can see that all couplings between qubits that are 3 sites apart have been eliminated. However, some terms that we want to keep, such as the nearest-neighbor coupling $\sigma_3^z \sigma_4^z$ and next-nearest coupling $\sigma_3^z \sigma_5^z$, are also eliminated. In order to make up for this problem, in phase 2 and 3 we use the same technique but shift the target qubits one site a time as shown in Fig. 3. This gives us the following effective Hamiltonian for these two phases

$$\begin{aligned} H_2^{eff} &= J_1(\sigma_2^z \sigma_3^z + \sigma_3^z \sigma_4^z + \sigma_5^z \sigma_6^z + \sigma_6^z \sigma_1^z) \\ &\quad + J_2(\sigma_2^z \sigma_4^z + \sigma_5^z \sigma_1^z) - B \sum_{i=1}^6 \sigma_i^x; \end{aligned} \quad (21)$$

$$\begin{aligned} H_3^{eff} &= J_1(\sigma_1^z \sigma_2^z + \sigma_3^z \sigma_4^z + \sigma_4^z \sigma_5^z + \sigma_6^z \sigma_1^z) \\ &\quad + J_2(\sigma_3^z \sigma_5^z + \sigma_6^z \sigma_2^z) - B \sum_{i=1}^6 \sigma_i^x. \end{aligned} \quad (22)$$

Obviously, the missing terms for nearest and next-nearest neighbor couplings in H_1^{eff} in Eq. (20) are compensated by remaining terms in Eqs. (21) and (22). Similarly, missing terms in H_2^{eff} and H_3^{eff} are compensated. Nevertheless, some next-nearest neighbor coupling terms are still missing from the sum of H_1^{eff} , H_2^{eff} and H_3^{eff} , since in each phase 2/3 of the nearest-neighbor couplings remain but only 1/3 of the next-nearest-neighbor couplings survive. In order to obtain all the nearest-neighbor and the next-nearest-neighbor couplings, we need a phase 4 as shown in Fig. 3. By keeping the next-nearest-neighbor interactions and eliminating the nearest-neighbor interactions, it gives us the effective Hamiltonian

$$\begin{aligned} H_4^{eff} &= J_2(\sigma_1^z \sigma_3^z + \sigma_2^z \sigma_4^z + \sigma_3^z \sigma_5^z + \sigma_4^z \sigma_6^z + \sigma_5^z \sigma_1^z + \sigma_6^z \sigma_2^z) \\ &\quad - B \sum_{i=1}^6 \sigma_i^x. \end{aligned} \quad (23)$$

The combined evolution of the system for the 4 phases

is

$$\begin{aligned} U &= U_4 U_3 U_2 U_1 \approx e^{-iH_4^{eff} 2\delta t} e^{-iH_3^{eff} 2\delta t} e^{-iH_2^{eff} 2\delta t} e^{-iH_1^{eff} 2\delta t} \\ &\approx e^{-i[H_4^{eff} + H_3^{eff} + H_2^{eff} + H_1^{eff}] 2\delta t} \\ &\triangleq e^{-iH_{eff} 8\delta t} \end{aligned} \quad (24)$$

where the effective average Hamiltonian is

$$\begin{aligned} H_{eff} &= \frac{1}{2} [J_1(\sigma_1^z \sigma_2^z + \sigma_2^z \sigma_3^z + \sigma_3^z \sigma_4^z + \sigma_4^z \sigma_5^z + \sigma_5^z \sigma_6^z + \sigma_6^z \sigma_1^z) \\ &\quad + J_2(\sigma_1^z \sigma_3^z + \sigma_2^z \sigma_4^z + \sigma_3^z \sigma_5^z + \sigma_4^z \sigma_6^z + \sigma_5^z \sigma_1^z + \sigma_6^z \sigma_2^z)] \\ &\quad - B \sum_{i=1}^6 \sigma_i^x. \end{aligned} \quad (25)$$

This is exactly the ANNNI model with periodic boundary condition.

Though we have used a 6-site chain to demonstrate how to eliminate couplings between qubits that are 3 sites apart, it is obvious that, by applying the operations $R_x^{(i,j,k)}(\pi)$ to groups of 3 qubits in the chain and shifting the target qubits by 1 site at a time in each phase, we can use the same technique to eliminate couplings between qubits 3 sites apart in an infinite-length spin chain. Notice that in Eq. (13) there are couplings between qubits 4 or more sites apart. These couplings are weaker since the interaction strengths λ^{j-1} in Eq. (13) decreases with the distance between qubits, but the error caused by them may still be unacceptable depending on the required accuracy of the simulation. By using a nested dynamical decoupling scheme, it can be shown that all couplings between qubits that are separated by 3 or more sites can be eliminated [29]. Therefore, given a required accuracy, we can in principle achieve the ANNNI Hamiltonian in Eq. (14).

IV. PHASE DIAGRAM OF THE ANNNI MODEL

Now that we can simulate the ANNNI model, we perform some analysis on its phase diagram. When $B = 0$ and λ is small, the nearest-neighbor interactions dominate and the ground state is the ferromagnetic state $|\downarrow\downarrow \cdots \downarrow\downarrow \cdots\rangle_z$ (or $|\uparrow\uparrow \cdots \uparrow\uparrow \cdots\rangle_z$). As λ increases, the next-nearest-neighbor interactions become important. When λ reaches some critical value, they become the dominating factor and the antiphase $|\uparrow\uparrow\downarrow\downarrow\uparrow\uparrow \cdots\rangle_z$ (or $|\downarrow\downarrow\uparrow\uparrow\downarrow\downarrow \cdots\rangle_z$) which minimizes the next-nearest neighbor interaction energy becomes the ground state. In the limit of large transverse field B , the ground state will be the paramagnetic phase $|\uparrow\uparrow \cdots \uparrow\uparrow \cdots\rangle_x$ to minimize the Zeeman energies.

From the above analysis, we see that there should be a ferromagnetic phase, a paramagnetic phase and an antiphase in the ANNNI model. However, there could be more subtle regimes in the phase diagram. Studies have shown (inconclusively) that there could be a unique floating phase in the deeply frustrated regime [18, 19]. This

phase is characterized by the fact that the n th-neighbor spin-spin correlation function in the longitudinal direction decays algebraically. The exact origin and range of the floating phase is still an open question and therefore a good subject for quantum simulation. Since the floating phase is located in the deeply frustrated regime, our circuit with strong couplings offers a good system for its simulation.

Many numerical recipes such as finite-size scaling method [17] and the interface approach [16] have been used to calculate the phase diagram of frustrated Ising model. We use the new method of time-evolving block decimation (TEBD) algorithm [30, 31] to calculate the ground state energy of ANNNI model. TEBD is a powerful algorithm to simulate quantum evolution process based on matrix product state and Trotter expansion [30, 31]. By making the evolution time imaginary, we get the so called i-TEBD which can be used to determine the ground state of a system efficiently. The TEBD method is based on the following matrix representation of a quantum state

$$|\Psi\rangle = \sum_{i_1=1}^d \cdots \sum_{i_n=1}^d c_{i_1 \dots i_n} |i_1\rangle \otimes \cdots \otimes |i_n\rangle \quad (26)$$

where d is the number of local energy levels on every site. The coefficients

$$c_{i_1 \dots i_n} = \sum_{\alpha_1, \dots, \alpha_{n-1}} \Gamma_{\alpha_1}^{[1]i_1} \xi_{\alpha_1}^{[1]} \Gamma_{\alpha_1 \alpha_2}^{[2]i_2} \xi_{\alpha_2}^{[2]} \Gamma_{\alpha_2 \alpha_3}^{[3]i_3} \cdots \Gamma_{\alpha_{n-1}}^{[n]i_n}. \quad (27)$$

are defined with the help of n tensors $\{\Gamma^{[1]}, \dots, \Gamma^{[n]}\}$ and $n-1$ vectors $\{\xi^{[1]}, \dots, \xi^{[n-1]}\}$, where χ is the maximal number of two-party Schmidt decomposition coefficients. In practice, χ does not need to be very large, because the Schmidt coefficients roughly decay exponentially with α . Any single-site operation or adjacent-site joined operation on the state can be achieved by updating the corresponding tensors and vectors. Here, we use the second order Trotter expansion for i-TEBD (see reference [31]).

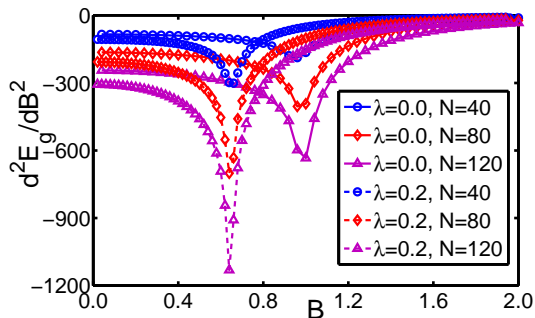


FIG. 4: (Color online) The finite-size scaling of second order derivative of ground state energy with $\lambda = 0$ (solid lines) and $\lambda = 0.2$ (dashed lines)

Using the TEBD algorithm, we calculate the ground state energy of ANNNI model in the external field B .

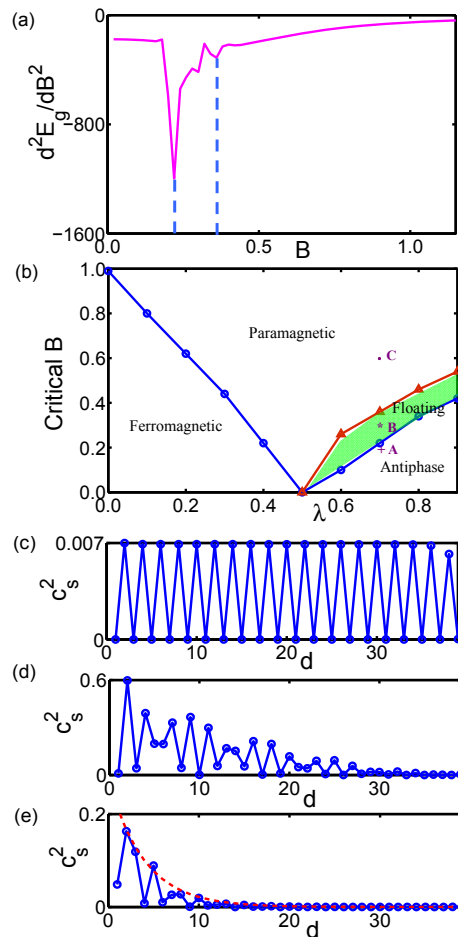


FIG. 5: (Color online) (a) Fine structures and small dips in the $d^2 E_g / dB^2$ curve with the parameters $\lambda = 0.7$ and $N = 60$. (b) The phase diagram of the ANNNI model. (c) The spin-spin correlation function $c_s^2(d)$ versus the spin separation d at point A ($\lambda = 0.7$ and $B = 0.2$) in the phase diagram. (d) $c_s^2(d)$ at point B ($\lambda = 0.7$ and $B = 0.3$) in the phase diagram. (e) $c_s^2(d)$ at point C ($\lambda = 0.7$ and $B = 0.6$) in the phase diagram.

How the ground state energy changes with the parameters in the Hamiltonian is of great significance because it gives us important clues on the quantum phase transition points. Considering this, we plot the second derivative of the ground state energy $d^2 E / dB^2$ in Fig. 4, for different coupling strength λ and system size N . Notice that there are dips in the curves in Fig. 4. Their positions nearly do not change with the system size N when N is large enough. These dips are where quantum phase transitions occur, and we can read from their positions the corresponding critical field strengths at the phase transition points. These critical parameter values allow us to construct the system's phase diagram which is shown in Fig. 5(b). The phase diagram is consistent with earlier results [19] obtained using different numerical methods.

Interestingly, as shown in Fig. 5(a) we find that in the strongly frustrated regime there can be a segment in the

curve of $d^2 E_g/dB^2$ where there are multiple extra small dips in addition to the main dip. This region is labeled by the green area in the phase diagram in Fig. 5(b). It is roughly at the location of the floating phase obtained in earlier work [19]. To further clarify the characteristics of the system in this region, we calculate the spin-spin correlation function

$$c_s(d) = \langle \sigma_{N/2+1}^z \sigma_{N/2+1+d}^z \rangle - \langle \sigma_{N/2+1}^z \rangle \langle \sigma_{N/2+1+d}^z \rangle. \quad (28)$$

in this region (point B in Fig. 5(b)) and compare it to the results in the antiphase and paramagnetic phase (point A and C in Fig. 5(b)). The results are plotted in Figs. 5(c), 5(d) and 5(e). As can be seen in the plots, the spin-spin correlation function at point A (Fig. 5(c)) exhibits perfect long-range order which is characteristic of the antiphase. At point C in the paramagnetic phase, the spin-spin correlation function (Fig. 5(e)) decays exponentially with spin separation. At point B in the green area in the phase diagram, the spin-spin correlation function (Fig. 5(d)) appears to decay algebraically which is indicative of the floating phase.

V. SIMULATING THE ANNNI MODEL IN THE SIX-JUNCTION ARRAY SYSTEM

The achievable scale of an experimental simulation system is limited, by both decoherence and the requirement for the two-level approximation to be valid (see appendix A). In order to study the feasibility of our Josephson circuit system for simulation of frustrated physics, we examine a small system to see how close its ground state is to certain phases in Fig. 5(b). This information will help us determine if it is possible to study the essential characteristics of a frustrated spin system using a quantum simulator of limited size.

Taking a 6-site Josephson junction array as an example, we obtain the ground state $|\psi\rangle_g$ of the corresponding $N = 6$ ANNNI model using exact diagonalization. Such a short chain is insufficient to exhibit the characteristics of the floating phase, therefore we will focus on the ferromagnetic, paramagnetic and antiphase phases. We calculate the probabilities of $|\psi\rangle_g$ being the ferromagnetic and paramagnetic states,

$$\begin{aligned} P(FM) &= |{}_g\langle\psi|\downarrow\downarrow\cdots\downarrow\downarrow\rangle_z|^2 + |{}_g\langle\psi|\downarrow\downarrow\cdots\downarrow\downarrow\rangle_x|^2, \\ P(PM) &= |{}_g\langle\psi|\uparrow\uparrow\cdots\uparrow\uparrow\rangle_x|^2. \end{aligned} \quad (30)$$

The results are plotted in Fig. 6 for different values of B and λ .

We can see in Fig. 6 that there exists a clear junction point $\lambda = 0.5$, which agrees well with the result in Fig. 5(b). If we associate the high probability regime with the corresponding phase, we can see that the phase regimes are nearly the same as well. This indicates that the 6-site example can already reveal some essential properties of the ANNNI model.

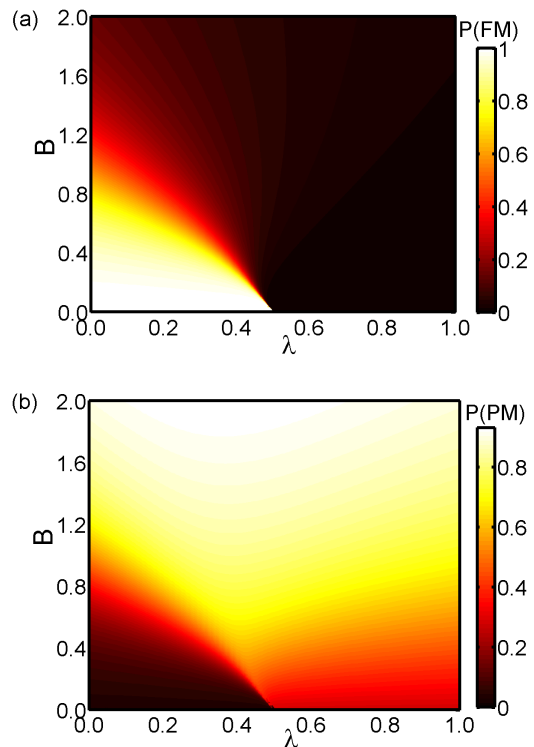


FIG. 6: (Color online) (a) The probability of the ground state $|\psi\rangle_g$ of the 6-site Josephson junction array being the ferromagnetic state. (b) The probability of $|\psi\rangle_g$ being the paramagnetic state.

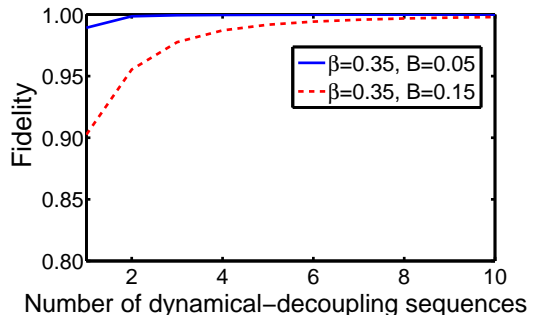


FIG. 7: The fidelity of the system state to the state of the corresponding ANNNI model, for different number of dynamical decoupling control sequences.

The results in Fig. 6 are based on exact diagonalization of the $N = 6$ ANNNI Hamiltonian. In order to obtain the ANNNI model from the Hamiltonian of the Josephson junction array, dynamical decoupling pulse sequences need to be applied to the qubits as shown in Fig. 3. To study the error of the pulse engineered ANNNI model, we evaluate the evolution of the Josephson junction array system in a time of $T = \pi$ under the control pulses, and compare it to that of a strict ANNNI model in the same amount of time. The initial state of the system is set to the maximal superposition state

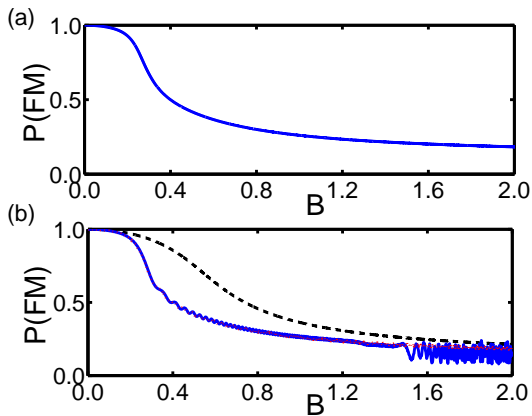


FIG. 8: (Color online) (a) Phase Transition process of the ANNNI model with $\lambda = 0.4$. (b) Phase transition process of the Josephson junction array system with and without the dynamical-decoupling control sequence. The black dashed curve is the result without dynamical-decoupling control sequences. The solid blue and dotted red curves are the results with 1 and 4 control sequences in unit time.

$|\Psi_0\rangle = \bigotimes_i (|\uparrow\rangle_i + |\downarrow\rangle_i)/\sqrt{2}$. We divide the total time T into m identical time interval: $T = m\delta t$. In each interval δt , the dynamical decoupling sequences shown in Fig. 3 are applied. In Fig. 7, the fidelities of the Josephson junction array system state compared to the state of the corresponding ANNNI model is plotted. We see that the fidelities increase with the number m of decoupling sequences, and they already reach 95% within a few sequences.

We can further evaluate the effectiveness of our pulse control scheme by comparing how the ground state changes with the external field B in a strict 6-site ANNNI model and in a pulse sequence controlled 6-site Josephson junction array. We simulate this process by adiabatically changing B in time and calculating the probability of the system ground state being in the ferromagnetic phase. Here, we set $\lambda = 0.4$. In Fig. 8(a), we calculate the state evolution of a 6-site ANNNI system initially in the ferromagnetic state $|\downarrow\downarrow\cdots\rangle_z$ when $B = 0$. We gradually increase the magnetic field B from 0 with velocity $v = 0.002$, and plot the probability that the system remains in the original ferromagnetic state at different values of B . We can see that when B becomes large, the system has deviated from the ferromagnetic state, indicating that it has changed to a different phase. In Fig. 8(b), we carry out the same study on the 6-site Josephson junction array under the control pulse scheme in Fig. 3. As can be seen, the probability of the system remains in the ferromagnetic state is almost identical to that in the corresponding ANNNI model when the number of control sequences is sufficient. These studies show that our control pulse based scheme can be used to accurately simulate the frustrated ANNNI model.

VI. CONCLUSION

In conclusion, we have shown how to simulate frustrated spin models using strongly coupled Josephson junction array. We find that the system Hamiltonian is exactly solvable beyond the small coupling limit, and we design a dynamical decoupling scheme to engineer the Hamiltonian for quantum simulation of the ANNNI model. We calculate the phase diagram of the system numerically using the TEBD method, and demonstrate that our control pulse based scheme can be used to simulate the corresponding ANNNI model accurately.

VII. ACKNOWLEDGMENT

This work was funded by National Natural Science Foundation of China (Grant Nos. 11174270, 60836001, 60921091), National Basic Research Program of China (Grant Nos. 2011CB921204, 2011CBA00200), the Fundamental Research Funds for the Central Universities (Grant No. WK2470000006), and Research Fund for the Doctoral Program of Higher Education of China (Grant No. 20103402110024). L. -H. Du and Z. -W. Zhou thank Man-Hong Yung for fruitful discussion. Z. -W. Zhou gratefully acknowledges the support of the K. C. Wong Education Foundation, Hong Kong.

Appendix A: Conditions for two-level approximation

In deriving the spin system Hamiltonian in Eq. (13), we used the two-level approximation for the Josephson qubits which kept only the $n_i = 0, 1$ states. We study the conditions for the two-level approximation to remain valid in this Appendix.

The Hamiltonian for the Josephson junction array system considering contributions from all charge states reads

$$\begin{aligned}
 H_n = & \frac{1}{\lambda} \sum_{i=1}^N (n_i - 1/2)^2 \\
 & + \sum_i \sum_{j=1}^2 (\lambda)^{j-1} (n_i - 1/2)(n_{i+j} - 1/2) \\
 & - B \sum_i \sum_n (|n\rangle_i \langle n+1| + h.c.), \quad (A1)
 \end{aligned}$$

where terms in the first line are the on-site charging energies of the Josephson qubits, terms in the second line are coupling energies between qubits, and terms in the third line are the Josephson tunneling energies. When the effective magnetic field B is nonzero, the Josephson tunneling energies can potentially cause leakage out of the $n_i = 0, 1$ states and invalidate the two-level approximation.

We take the ferromagnetic phase of the ANNNI model as an example to estimate the probability for the qubits

in the system to escape the $n_i = 0, 1$ states. Initially, assume $B = 0$ and the system is in the ferromagnetic state $|\Psi\rangle_g = |0101\dots\rangle$ (recall that there has been a canonical transformation applied on the even sites.). When B increases, the qubits can make transitions out of the $n_i = 0, 1$ states. We examine the system states that result when one of the qubits originally in the $n = 1$ state changes to the $n = 2$ state, because they are closest to $|\Psi\rangle_g$ in energy among all states that violate the two-level approximation. We denote such states $|\Psi\rangle_n$. Their energies differ from that of $|\Psi\rangle_g$ by $\Delta E = 2(1/\lambda - 1 + \lambda)$ according to Eq. (A1).

According to the first order perturbation theory, the ground state with a nonzero magnetic field is

$$\begin{aligned} |\Psi'\rangle_g &= |\Psi\rangle_g + \sum_n \frac{\langle\Psi|H'|\Psi\rangle_g}{E_g - E_n} |\Psi\rangle_n \\ &= |\Psi\rangle_g + \frac{B}{\Delta E} (\sum_n |\Psi\rangle_n). \end{aligned} \quad (\text{A2})$$

With the form of $|\Psi'\rangle_g$, the total escaping probability out of the $n_i = 0, 1$ Hilbert subspace can be estimated to be

$$P_{esc} = \left(\frac{B}{\Delta E}\right)^2 \frac{N}{2}, \quad (\text{A3})$$

where the factor of N is due to the translational symmetry.

From the Eq. (A3), we find that the escaping probability is proportional to N . Therefore the allowable system size N is limited by the tolerable escaping probability and the amplitude of the magnetic field. For example, if an escaping probability of 5% is acceptable, and $B = 0.2$, the allowable size of the Josephson junction array is about $N = 10$.

-
- [1] D. Jaksch, P. Zoller, *Ann. Phys.* **315**, 52 (2005).
[2] I. Buluta and F. Nori, *Science* **326**, 108 (2009).
[3] A. Micheli, G. K. Brennen and P. Zoller, *Nat. Phys.* **2**, 341 (2006).
[4] S. L. Sondhi, S. M. Girvin, J. P. Carini and D. Shahar, *Rev. Mod. Phys.* **69**, 315 (1997).
[5] J. Q. You, X. F. Shi, X. Hu, and F. Nori, *Phys. Rev. B* **81**, 014505 (2010).
[6] I. Bloch, T. W. Hänsch and T. Esslinger, *Nature* **403**, 166 (2000).
[7] J. K. Chin, D. E. Miller, Y. Liu, C. Stan, W. Setiawan, C. Sanner, K. Xu and W. Ketterle, *Nature* **443**, 689 (2008).
[8] J. Simon, W. S. Bakr, R. Ma, M. E. Tai, P. M. Preiss, and M. Greiner, *Nature* **472**, 307 (2011).
[9] J. Struck, C. Ölschläger, R. Le Targat, P. Soltan-Panahi, A. Eckardt, M. Lewenstein, P. Windpassinger, and K. Sengstock, *Science* **333**, 996 (2011).
[10] A. Friedenauer, H. Schmitz, J. T. Glückert, D. Porras, T. Schätz, *Nat. Phys.* **4**, 757 (2008).
[11] K. Kim, M. S. Chang, S. Korenblit, R. Islam, E. E. Edwards, J. K. Freericks, G. D. Lin, L. M. Duan and C. Monroe, *Nature* **465**, 590 (2010).
[12] Y. Hu, Z. W. Zhou and G. C. Guo, *New. J. Phys.* **9**, 27 (2007).
[13] S. Rebić and J. Twamley, and G. J. Milburn, *Phys. Rev. Lett.* **103**, 150503 (2009).
[14] L. Tian, *Phys. Rev. Lett.* **105**, 167001 (2010).
[15] C. Arizmendi, A. Rizzo, L. Epele, and C.G. Canal, *Z. Phys. B: Condens. Matter* **83**, 273 (1991).
[16] P. Sen, *Phys. Rev. B* **55**, 11367 (1997).
[17] Paulo R. Colares Guimarães, J. A. Plascak, F. C. Sá Barreto and J. Florencio, *Phys. Rev. B* **66**, 064413 (2002).
[18] A. K. Chandra, and S. Dasgupta, *Phys. Rev. E* **75**, 021105 (2007).
[19] M. Beccaria, M. Campostrini, and Alessandra Feo, *Phys. Rev. B* **76**, 094410 (2007).
[20] M. Tinkham, *Introduction to superconductivity*, (McGraw-Hill, Inc. New York, 1996).
[21] J. Q. You, X. Hu, and Franco Nori, *Phys. Rev. B* **72**, 144529 (2005).
[22] Nakamura, Y., Y. A. Pashkin, and J. S. Tsai, *Nature* **398**, 786 (1999).
[23] Y. Makhlin, G. Schön, and A. Shnirman, *Rev. Mod. Phys.* **73**, 357 (2001).
[24] Yu. A. Pashkin, O. Astafiev, T. Yamamoto, Y. Nakamura, and J. S. Tsai, *Quantum Inf. Proc.* **8**, 55 (2009).
[25] M. E. Fisher, and W. Selke, *Phys. Rev. Lett.* **44**, 1502 (1980).
[26] W. Selke, *Phys. Rep.* **170**, 213 (1988).
[27] L. Viola and S. Lloyd, *Phys. Rev. A* **58**, 2733 (1998).
[28] L. Viola, E. Knill, and S. Lloyd, *Phys. Rev. Lett.* **82**, 2417(1999).
[29] L. Du, et al. unpublished.
[30] G. Vidal, *Phys. Rev. Lett.* **91**, 147902 (2003)
[31] G. Vidal, *Phys. Rev. Lett.* **93**, 040502 (2004).